Earthq Eng & Eng Vib (2023) 22: 1031-1043 **DOI**: https://doi.org/10.1007/s11803-023-2213-9

Smartphone-based bridge frequency identification using vehicle contact-point response

Liu Chengyin†, Zhu Yipeng‡, Zeng Qing§ and Wu Xiaodong‡

Shenzhen Key Laboratory of Intelligent Structure System in Civil Engineering, Harbin Institute of Technology, Shenzhen 518055, China

Abstract: Bridge frequency (BF) identification using the vehicle scanning method has attracted considerable attention during the last two decades. However, most previous studies have adopted unrealistic vehicle models, thus finding limited practical applications. This study proposes a smartphone-based BF identification method that uses the contact-point acceleration response of a four degree-of-freedom vehicle model. The said response can be inferred from the vehicle body response measured by a smartphone. For realizing practical applications, this method is incorporated into a self-developed smartphone app to obtain data smoothly and identify BFs in a timely manner. Numerical and experimental investigations are performed to verify the effectiveness of the proposed method. In particular, the robustness of this method is investigated numerically against various factors, including the vehicle speed, bridge span, road roughness, and bridge type. Furthermore, laboratory calibration tests are performed to investigate the accuracy of the smartphone gyroscope in measuring the angular velocity, where anomalous data are detected and eliminated. Laboratory experiment results for a simply supported bridge indicate that the proposed method can be used to identify the first two BFs with acceptable accuracy.

Keywords: bridge frequency (BF) identification; vehicle–bridge interaction; four degree-of-freedom (DOF) vehicle model; contact-point response; smartphone

1 Introduction

Bridge frequency (BF) is an important modal parameter for structural health monitoring of bridges and is widely used for updating finite element models and detecting structural damage. Conventionally, sensors, such as accelerometers, are installed at key locations of a bridge to acquire structural responses under external excitations, following which the BFs can be extracted through Fourier spectrum analysis (Yang and Chang, 2009). However, this type of direct method is generally not cost-effective because the on-site instrumentation of the bridge is costly, risky, time-consuming, and not long-lasting (Yang *et al*., 2019a, 2019b).

Correspondence to: Zeng Qing, School of Civil and Environment Engineering, Harbin Institute of Technology, Shenzhen 518055, China
Tel: +86-13163774176
E-mail: zengqing@hit.edu.cn
†Associate Professor; ‡PhD Candidate; §Assistant Professor

Supported by: National Natural Science Foundation of China under Grant Nos. 51978215 and 52378295, National Key R&D Program of China under Grant No. 2019YFC1511100, Guangdong Basic and Applied Basic Research Foundation under Grant No. 2022A1515110587, and Shenzhen S&T Project under Grant Nos. JCYJ20200109112816582 and KQTD20210811090112003

Received November 3, 2021; **Accepted** April 15, 2023

To this end, in 2004, Yang *et al*. (2004) developed the vehicle scanning method (VSM), a type of indirect monitoring method, to enable practical measurements of the fundamental frequency of medium- and short-span bridges. This method formulates a vehicle as a sprung mass with a single degree-of-freedom (DOF) and aims to capture meaningful structural information from its vibration responses during vehicle-bridge interaction (VBI). In comparison with direct methods, the VSM offers advantages, such as economy, efficiency, and mobility (Yang and Yang, 2018; Shokravi *et al*., 2020). Following a preliminary study, the VSM was further validated through a series of field experiments (Lin and Yang, 2005; Yang *et al*., 2013a), and the findings obtained were expanded upon by several subsequent studies. For example, Cantero *et al*. (2017) performed field tests to investigate the evolution of the modal properties (i.e., vibration modes) of a bridge during the passage of a truck simulated as a single-DOF spring-mass system. Furthermore, they experimentally identified the nonstationary and nonlinear features of vehicle responses from a scaled VBI laboratory test bed (Cantero *et al*., 2019). The Hilbert transform (HT) approach has a promising capacity to determine modal parameters of structures (Chen and Feng, 2003; Nagarajaiah and Basu, 2009). Based on HT combined with other techniques, Han *et al*. (2014) proposed methods of modal identification and damage diagnosis,

such as random decrement technique (RDT), natural excitation technique (NExT) and stochastic subspace identification (SSI). Li *et al*. (2019a) proposed to estimate the BF from the dynamic responses of two vehicles using an SSI technique wherein one vehicle served as a fixed reference sensor and the other served as a moving sensor. To eliminate the effect of road roughness during BF extraction, Yang *et al*. (2012) used two connected vehicles with identical properties to reduce the surface roughness effect by subtracting the spectral response of the following vehicle from the leading vehicle. Overall, previous studies mainly modeled vehicles as a single-DOF or single-axle system (Yang *et al*., 2004; Cantero *et al*., 2017; Han *et al*., 2014; Li *et al*., 2019a) and may have therefore oversimplified and limited the practical implementation of the VSM for BF identification, as highlighted in a recent review by Yang *et al*. (2020a). Therefore, to supplement the VSM theory and enhance its applicability, Yang *et al*. (2019c) developed a theoretical framework to investigate the dynamic response of a two-axle asymmetric vehicle (two-DOF) moving over a bridge. Very recently, Jin *et al*. (2021) developed a short-time SSI framework for estimating BFs using the dynamic response of a traversing vehicle, in which a more realistic multi-DOF vehicle model was considered.

Notably, the obtained vehicle response commonly contains not only the BF of interest but also the vehicle frequency and driving frequency (Li *et al*., 2019a, 2019b). As a result, the BF may become imperceptible. To address this concern, Yang *et al*. (2013b) compared the performance of three techniques for vehicle-frequency filtering — band-pass filter (BPF), singular spectrum analysis (SSA), and singular spectrum analysis with band-pass filter (SSA-BPF). Among these, the SSA-BPF demonstrates the best performance. Moreover, Yang *et al*. (2018) proposed a unique method of using the acceleration response of the contact point (CP) between the vehicle (single-DOF) and bridge for BF measurement, because it is independent of the vehicle frequency. Furthermore, field-investigation results obtained using a self-designed two-wheel trailer demonstrated that CP response was superior to vehicle (body) responses in detecting the first few BFs (Yang *et al*., 2020b). Another study (Yang *et al*., 2019c) further derived the CP response between a two-axle vehicle (two-DOF) and a bridge, and proved that it is an excellent parameter for BF extraction.

Recently, there has been a surge in the development of techniques that leverage smartphone technology for mobile sensing of civil infrastructures. This is because modern-day smartphones are commonly equipped with several advanced sensors, such as accelerometers, magnetometers, and gyroscopes. Such smartphones afford new possibilities with regard to VSM development. When mounted on a vehicle, smartphones can not only act as sensors for data collection/transfusion but also process data in a timely manner when the vehicle passes over a bridge (Matarazzo *et al*., 2018). Consequently, the utility of a smartphone-based VSM can be extended to monitor a large number of bridges using the internet of vehicles and augmented via installation of a large number of smartphones on vehicles (i.e., crowdsensing) (Mei and Gül, 2019a, Mei *et al*.,2019b, 2020). Thus, the operational behavior of a bridge can be regularly monitored to track its condition, thereby improving the efficiency of its management. In this regard, Matarazzo *et al*. (2018) conducted field tests for measuring BFs using vehicle-mounted smartphones and demonstrated that the acceleration data collected could be used for capturing the first few BFs. Similarly, Shirzad-Ghaleroudkhani and Gül (2020) proposed a methodology that used an inverse filtering technique to extract BFs from acceleration signals recorded by passing smartphone-equipped vehicles. In particular, they used the off-bridge signal spectrum to design a specific inverse filter and applied the same to on-bridge data. Their laboratory experiment results revealed their proposed filter design to suppress vehicle frequencies and amplify BF. Moreover, Shirzad-Ghaleroudkhani *et al*. (2020) demonstrated that a large number of smartphone-equipped vehicles (simulated as different combinations of mass and suspension springs as well as operating speeds) could capture fundamental BFs.

The above review suggests that existing VSMs can be used to identify the first few BFs of interest. In addition, the vehicle models adopted in most previous studies are single-axle vehicle models which do not reflect the actual vehicle movement. Therefore, the development of a more accurate vehicle model that can reflect the dynamic properties of actual vehicles is of utmost importance. To this end, the present study proposes a low-cost smartphone-based BF identification method that uses the CP response of a two-axle vehicle model (four-DOF), which can be inferred from the vehicle body response measured by a smartphone. The two-axle vehicle model can more realistically reflect the actual road surface conditions by considering the pitching effect (Yang *et al.*, 1999, 2022), and a smartphone can conveniently measure the angular velocity of the vehicle pitching motion. This method first obtains the CP response and then derives the BF through a Fourier transform. As a practical implementation, this method is incorporated into a self-developed smartphone app to obtain the BF conveniently through a smartphone mounted in a vehicle as it passes over a bridge.

The remainder of this paper is organized as follows. Section 2 describes the use of the CP acceleration response of a four-DOF vehicle model for BF identification. Section 3 presents the numerical verification of the proposed method as well as the results of an extensive parametric study. Section 4 discusses the laboratory experiments performed to demonstrate the effectiveness of the developed method. Finally, Section 5 presents the conclusions drawn from this study.

2 Proposed method for BF identification

Herein, Section 2.1 describes the theoretical formulation of a closed-form solution of the CP displacement response for a four-DOF vehicle model. Then, Section 2.2 establishes a relationship between the CP acceleration and the vehicle body response to facilitate BF identification.

2.1 CP response of four-DOF vehicle

Figure 1 depicts the VBI model used in this study. The two-axle vehicle moving at speed v has four DOFs: vehicle body vertical movement z, vehicle pitch motion θ, and vertical movements of two wheels z_1 and z_2. A sensor (e.g., smartphone) is installed on the vehicle body to obtain its response as it passes over a bridge. The bridge is modeled as a simply supported beam of length L with a smooth surface.

The equation of motion (EOM) for the beam with the damping effect being neglected is

$$\bar{m}\ddot{u} + EI\frac{\partial^4 u}{\partial x^4} = F(t) \tag{1}$$

where, $\bar{m}$ denotes the unit mass; E, the elastic modulus; I, the moment of inertia; and u, the vertical displacement of the beam. For the sake of an analytical derivation, the action of the vehicle on the beam can be considered as two discrete moving loads (Yang and Yau, 2015; Yang *et al*., 2019c), neglecting the vehicle′s inertial effect; i.e.,

$$F(t) = \sum_{k=1}^{2} p_k \delta\left[x - v(t - t_k)\right]\left[H(t - t_k) - H(t - t_k - \Delta t)\right] \tag{2}$$

and

$$p_k = \frac{d - d_k}{d} m_v g + m_k g,\ \Delta t = \frac{L}{v},\ t_k = \frac{(k-1)d}{v} \tag{3}$$

where, δ is the Dirac delta function; H, the unit step function; d, the distance between the front and rear axles; p_k, the load from the kth axle (k = 1, 2); t_k, the entrance time for the kth axle to the beam; g, the acceleration due to gravity; and d_k, the distance between the kth axle and vehicle center of gravity. Furthermore, m_v and m_k denote the vehicle and k th-wheel masses, respectively.

According to the modal superposition method, the vertical displacement of a simply supported beam is given by

$$u = \sum_{n=1}^{N}\left[q_{bn}(t)\sin\frac{n\pi x}{L}\right] \tag{4}$$

where, $\sin(n\pi x / L)$ and $q_{bn}(t)$ represent the modal shape and modal coordinate, respectively.

By substituting Eq. (4) into Eq. (1) and for zero initial conditions, the beam vertical displacement u can be obtained by solving Eq. (1).

$$u(x,t) = \sum_{n=1}^{N}\sum_{k=1}^{2} A_n p_k \left\{\left[\sin\frac{n\pi v(t - t_k)}{L} - S_n \sin w_{bn}(t - t_k)\right]H(t - t_k) + \left[\sin\frac{n\pi v(t - t_k - \Delta t)}{L} - S_n \sin w_{bn}(t - t_k - \Delta t)\right]H(t - t_k - \Delta t)\right\}\sin\frac{n\pi x}{L} \tag{5}$$

where

$$w_{bn} = \frac{n^2\pi^2}{L^2}\sqrt{\frac{EI}{\bar{m}}},\ A_n = -\frac{2L^3}{EIn^4\pi^4(1 - S_n^2)},\ S_n = \frac{n\pi v}{L w_{bn}} \tag{6}$$

The coordinate of each CP is

$$x = v(t - t_k) \tag{7}$$

By substituting Eq. (7) into Eq. (5) and using trigonometric properties, the CP displacement of the front and rear wheels can be solved as

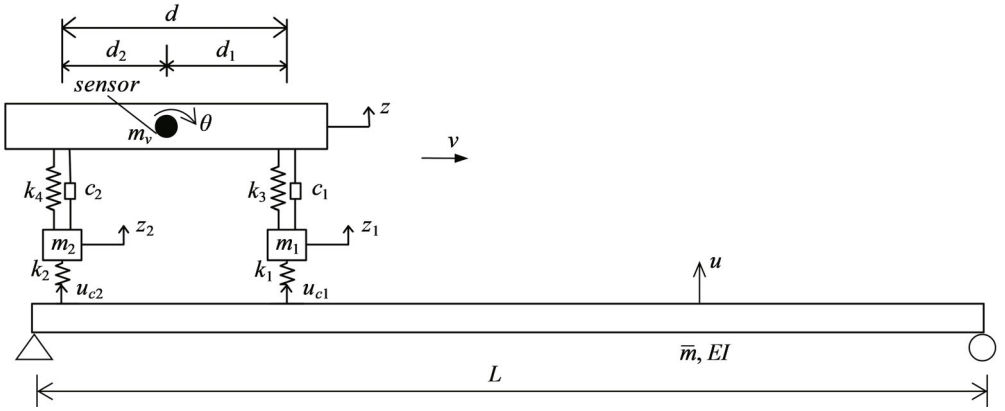

Fig. 1 VBI model considered in this study

$$u_{cR}=\sum_{n=1}^{N}\sum_{k=1}^{2}A_n p_k \frac{1}{2}\left\{\left\{-\cos\left(\frac{2n\pi v}{L}t-\theta_{n1}\right)+\cos\frac{n\pi v\left(t_R-t_k\right)}{L}+ S_n\cos\left[\left(w_{bn}+\frac{n\pi v}{L}\right)t-\theta_{n2}\right]-S_n\cos\left[\left(w_{bn}-\frac{n\pi v}{L}\right)t+\theta_{n3}\right]\right\}H\left(t-t_k\right)+ \left\{-\cos\left(\frac{2n\pi v}{L}t-\theta_{n4}\right)+\cos\frac{n\pi v\left(t_R-t_k-\Delta t\right)}{L}+ S_n\cos\left[\left(w_{bn}+\frac{n\pi v}{L}\right)t-\theta_{n5}\right]-S_n\cos\left[\left(w_{bn}-\frac{n\pi v}{L}\right)t+\theta_{n6}\right]\right\}H\left(t-t_k-\Delta t\right)\right\},\quad R=1,\ 2 \tag{8}$$

where the phase angles are

$$\theta_{n1}=\frac{n\pi v}{L}\left(t_R+t_k\right),\ \theta_{n2}=\frac{n\pi v}{L}t_R+w_{bn}t_k,\quad \theta_{n3}=\frac{n\pi v}{L}t_R-w_{bn}t_k,\ \theta_{n4}=\frac{n\pi v}{L}\left(t_R+t_k+\Delta t\right),\quad \theta_{n5}=\frac{n\pi v}{L}t_R+w_{bn}\left(t_k+\Delta t\right),\ \theta_{n6}=\frac{n\pi v}{L}t_R-w_{bn}\left(t_k+\Delta t\right) \tag{9}$$

As indicated in Eq. (8), the CP displacement is dominated by three frequency components: the driving frequency $2n\pi v/l$ induced by the vehicle movement, left-shifted frequency of the beam $w_{bn}-n\pi v/l$, and right-shifted frequency of the beam $w_{bn}+n\pi v/l$. This also confirms that the CP displacement is independent of the vehicle frequency and lays the foundation for the proposed method discussed later on that the CP response contains the information to identify BF. This finding is consistent with those obtained by modeling the vehicles as a single-DOF (Yang *et al*., 2018) and two-DOF system (Yang *et al.*, 2019c).

2.2 BF identification based on CP acceleration response

Figure 2 shows a schematic diagram of the adopted four-DOF vehicle model, for which the CP acceleration response can be derived indirectly based on the measured vertical acceleration and rotational angular acceleration at the center of gravity of the vehicle, $\ddot{z}$ and $\ddot{\theta}$, respectively. The vertical movements z_3 and z_4 of the two points A and B on the vehicle body above the CPs can be calculated as $z_3=z-d_1\theta$ and $z_4=z+d_2\theta$, respectively (Paraskeva *et al*., 2017).

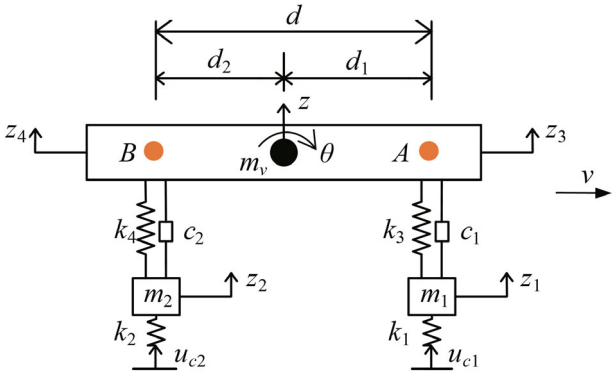

Fig. 2 Four-DOF vehicle model

The governing equations for the four-DOF vehicle can be defined with respect to the static equilibrium position as

$$m_v\ddot{z}+c_1\left(\dot{z}-d_1\dot{\theta}-\dot{z}_1\right)+c_2\left(\dot{z}+d_2\dot{\theta}-\dot{z}_2\right)+k_3\left(z-d_1\theta-z_1\right)+k_4\left(z+d_2\theta-z_2\right)=0 \tag{10a}$$

$$I_v\ddot{\theta}+d_2c_2\left(\dot{z}+d_2\dot{\theta}-\dot{z}_2\right)+d_2k_4\left(z+d_2\theta-z_2\right)-d_1k_3\left(z-d_1\theta-z_1\right)-d_1c_1\left(\dot{z}-d_1\dot{\theta}-\dot{z}_1\right)=0 \tag{10b}$$

$$m_1\ddot{z}_1-k_3\left(z-d_1\theta-z_1\right)-c_1\left(\dot{z}-d_1\dot{\theta}-\dot{z}_1\right)+k_1\left(z_1-u_{c1}\right)=0 \tag{10c}$$

$$m_2\ddot{z}_2-k_4\left(z+d_2\theta-z_2\right)-c_2\left(\dot{z}+d_2\dot{\theta}-\dot{z}_2\right)+k_2\left(z_2-u_{c2}\right)=0 \tag{10d}$$

where, I_v denotes the moment of inertia of the vehicle body; k_1, k_2, k_3, and k_4 are the stiffness of the front wheel, rear wheel, front suspension, and rear suspension, respectively; c_1 and c_2 are the damping coefficients of the front suspension and rear suspension, respectively; and u_{c1} and u_{c2} are the vertical displacements at the two CPs, respectively.

The double differentiation of Eqs. (10a) and (10b) yields

$$c_1\dddot{z}_1+c_2\dddot{z}_2+k_3\ddot{z}_1+k_4\ddot{z}_2=m_v\dddot{z}+\left(c_1+c_2\right)\ddot{z}+\left(c_2d_2-c_1d_1\right)\dddot{\theta}+\left(k_3+k_4\right)\dot{z}+\left(k_4d_2-k_3d_1\right)\ddot{\theta} \tag{11a}$$

$$d_2c_2\dddot{z}_2-d_1c_1\dddot{z}_1+d_2k_4\ddot{z}_2-d_1k_3\ddot{z}_1=I_v\ddddot{\theta}+\left(d_2c_2-d_1c_1\right)\dddot{z}+\left(d_2^2c_2+d_1^2c_1\right)\dddot{\theta}+\left(d_2k_4-d_1k_3\right)\ddot{z}+\left(d_2^2k_4+d_1^2k_3\right)\ddot{\theta} \tag{11b}$$

In Eq. (11), the two right-hand-side terms (represented by F_1 and F_2) can be considered as time-series expressions, whereas terms $\dddot{z}$ and $\ddot{z}$ can be replaced by the difference quotients expressed as

$$\dddot{z}=\frac{\ddot{z}\left(i+1\right)-2\ddot{z}\left(i\right)+\ddot{z}\left(i-1\right)}{\left(\Delta t\right)^2} \tag{12a}$$

$$\ddot{z}=\frac{\dot{z}\left(i+1\right)-\dot{z}\left(i\right)}{\Delta t} \tag{12b}$$

where Δt denotes the sampling interval and i denotes the i th sampling point.

By solving Eq. (11), the wheel response can be expressed as

$$\dddot{z}_1 = \frac{d_2 F_1 - F_2 - dk_3 \ddot{z}_1}{dc_1} \tag{13a}$$

$$\dddot{z}_2 = \frac{d_1 F_1 + F_2 - dk_4 \ddot{z}_2}{dc_2} \tag{13b}$$

where $\ddot{z}_1$ and $\ddot{z}_2$ stand for the acceleration responses of the front and rear wheels, respectively. These can be solved using the improved Euler method because Eq. (13) can be treated as a first-order ordinary differential equation.

Following the second-order differentiation of Eqs. (10c) and (10d), the CP acceleration responses can be expressed as

$$\ddot{u}_{c1} = \frac{m_1 \dddot{z}_1 - c_1\left(\dddot{z} - d_1\dddot{\theta} - \dddot{z}_1\right) - k_3\left(\ddot{z} - d_1\ddot{\theta} - \ddot{z}_1\right)}{k_1} + \ddot{z}_1 \tag{14a}$$

$$\ddot{u}_{c2} = \frac{m_2 \dddot{z}_2 - c_2\left(\dddot{z} + d_2\dddot{\theta} - \dddot{z}_2\right) - k_4\left(\ddot{z} + d_2\ddot{\theta} - \ddot{z}_2\right)}{k_2} + \ddot{z}_2 \tag{14b}$$

Consequently, as long as the vehicle body responses have been obtained, the CP acceleration response can be calculated using Eq. (14). In this study, the discrete Fourier transform (DFT) method is used to perform frequency domain analysis of the derived CP acceleration responses as it can make full use of each discrete data point inside the signal. To eliminate the effect of road roughness in BF identification, Yang *et al*. (2012) proposed to subtract the acceleration Fourier spectrum of two connected vehicles. Inspired by this idea, this study proposes to subtract the CP acceleration Fourier spectrum of the front and rear wheels and to identify the BF from the residual spectrum. The effectiveness of using the CP acceleration response for BF identification is validated in the sections below.

To facilitate data collection and processing, the proposed VSM for BF identification is incorporated into a self-developed Android smartphone app. As a result, a smartphone mounted at the center of the vehicle body can be used to measure the vertical acceleration and pitch angular velocity responses of the vehicle continuously as it passes over a bridge. Furthermore, it can be used to analyze the signal in a timely manner and identify BFs when the vehicle ends its trip.

3 Numerical simulation

To investigate the feasibility and effectiveness of the proposed method for BF identification, numerical simulations of the VBI system (see Fig. 1) are performed, and the accuracy of the proposed method in both calculating the CP response and identifying BFs is validated. Notably, in practice, the BF identification performance may be affected by diverse factors, such as the vehicle movement speed, bridge span, road roughness, and bridge type. To determine the feasibility of the proposed method, these factors are evaluated independently by varying them while maintaining the others constant.

3.1 BF identification using proposed method

Tables 1 and 2, respectively, list the properties of the bridge and vehicle models used in this study. The vehicle movement speed was maintained constant at 5 m/s. The damping matrix of the bridge is assumed to be of the Rayleigh type and calculated by setting the damping ratios of the first two modes to be 0.02.

Different from the derivation in Section 2.1, the numerical simulation herein models the bridge with the finite element BEAM188 with the help of the available commercial platform ANSYS (ANSYS, 2021). The multibody vehicle model is simulated with the MASS21 element connected by the COMBIN14 element representing the suspension system. The numerical analysis models the VBI with the elastic contact, denoted as k_1 and k_2. Two massless CPs with the DOFs of u_{c1} and u_{c2} are rigidly attached to the bridge element by the MPC184 element. The Newmark-β method integrates the VBI system′s EOM using the pertinent parameters $\gamma = 1/2$ and $\beta = 1/4$. The time step is 0.0025 s. The accordance between the standard VBI analysis (Paraskeva *et al*., 2017; Zeng *et al*., 2022) and the proposed method in ANSYS verifies the validity.

As seen in Eq. (14) in Section 2.2, the CP acceleration responses are uniquely determined from the car body

Table 1 Bridge model properties

Parameter	L (m)	$\bar{m}$ (kg/m)	E (Pa)	I (m^4)
Value	25	2000	2.75×10^{10}	0.15

Table 2 Vehicle model properties

Parameter	Value	Parameter	Value
m_v (kg)	690	k_3 (N/m)	17000
I_v (kg·m^2)	1222	k_4 (N/m)	22000
m_1 (kg)	40.5	c_1 (N·s/m)	1500
m_2 (kg)	45.4	c_2 (N·s/m)	1500
k_1 (N/m)	192000	d_1 (m)	1.3
k_2 (N/m)	192000	d_2 (m)	1.5

responses, i.e., the vertical acceleration and the rotational angular acceleration. Therefore, the pertinent vehicle body responses are extracted from the VBI response and work as the artificial excitation inputs to formulate indirectly the CP accelerations by eliminating the bridge system (see Eq. (14)). Note that these artificial vehicle body responses will be updated with practical field measurement instead in the experiment setup in Section 4. The CP accelerations are further compared with those calculated directly from VBI analysis in ANSYS, as shown in Fig. 3(a). The two curves agree well with each other, thereby indicating that the derived CP acceleration response is reliable and may be used for subsequent BF identification. Figure 3(b) shows the CP acceleration spectrum acquired through DFT, from which the first four BFs (ω_{b1}, ω_{b2}, ω_{b3}, and ω_{b4}) could be identified clearly with errors within 7% (see Table 3). Therefore, the proposed BF identification method is effective and provides results with sufficient accuracy.

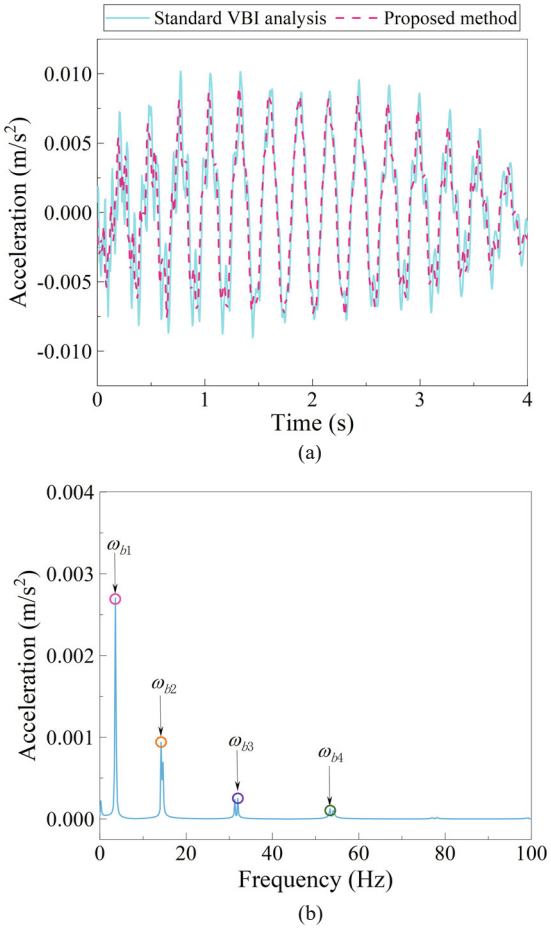

Fig. 3 (a) Comparison of CP acceleration responses and (b) CP acceleration spectrum

3.2 Parametric study

3.2.1 Effect of vehicle speed

As noted above, the first four BFs for the test vehicle moving at 5 m/s could be identified accurately. To investigate the effect of vehicle speed on the BF identification results, vehicle speeds of 2 m/s and 8 m/s were also tested; in particular, a higher vehicle speed would reduce the accuracy of indirect bridge modal identification by reducing the length of the obtained signals (Jian *et al*., 2020). Table 4 lists the identified BFs under each vehicle speed. All errors were smaller than 8%, indicating that the vehicle speed had little effect on BF identification using the proposed method.

3.2.2 Effect of bridge span

To study the effect of bridge span on the BF identification results, a simply supported bridge with spans of 20, 30, and 40 m was investigated; Table 5 lists the obtained results. The BF identification accuracy seemingly improved with increasing bridge span. This is mainly because for a test vehicle with constant speed and sampling frequency, the length of the obtained signals is proportional to the bridge span. In other words, more BF components would be involved in the CP responses for a bridge with a longer span. However, the error of the identified 4th BF for a bridge span of 20 m was ~14%, which is considerably high. This suggests that the proposed approach is more suitable for a simply supported bridge with a span longer than 20 m.

3.2.3 Effect of road roughness

The road roughness is well recognized to be one of the major obstacles in successful BF identification using a VSM (Yang *et al*., 2020a). To verify the effectiveness of the proposed method in eliminating the effect of road roughness, three classes of road roughness profile $r(x)$ were generated using the power spectral density function provided in ISO 8608 (ISO-8608, 1995): Class A (best), Class B (very good), and Class C (good). The

Table 3 Comparison of identified and theoretical BFs (unit: Hz)

BF	Identified	Theoretical	Error
1st BF	3.602	3.610	0.22%
2nd BF	14.405	14.438	0.23%
3rd BF	31.625	32.485	2.65%
4th BF	53.800	57.751	6.84%

Table 4 Identified BFs under various vehicle speeds (unit: Hz)

Speed	1st BF	Error of 1st BF	2nd BF	Error of 2nd BF	3rd BF	Error of 3rd BF	4th BF	Error of 4th BF
2 m/s	3.603	0.19%	14.410	0.19%	31.610	2.69%	53.770	6.89%
8 m/s	3.600	0.28%	14.400	0.26%	31.680	2.48%	53.650	7.10%

road roughness is incorporated in the ANSYS modeling as external excitation to both the vehicle wheels and the bridge system, which is calculated as the product of its magnitude and the contact stiffness k_1 and k_2. Figures 4(a), 4(b), and 4(c) show plots of the CP acceleration residual spectra corresponding to these three classes of road roughness, respectively. The first four BFs (ω_{b1}, ω_{b2}, ω_{b3}, and ω_{b4}) were identified with satisfactory accuracy in all cases, implying that the effect of road roughness was eliminated successfully.

Table 5 Errors of identified BFs for various simply supported bridge spans

Bridge span	1st BF	2nd BF	3rd BF	4th BF
20 m	2.15%	2.12%	5.86%	14.05%
30 m	2.59%	0.84%	1.44%	3.79%
40 m	0.07%	0.16%	0.46%	1.41%

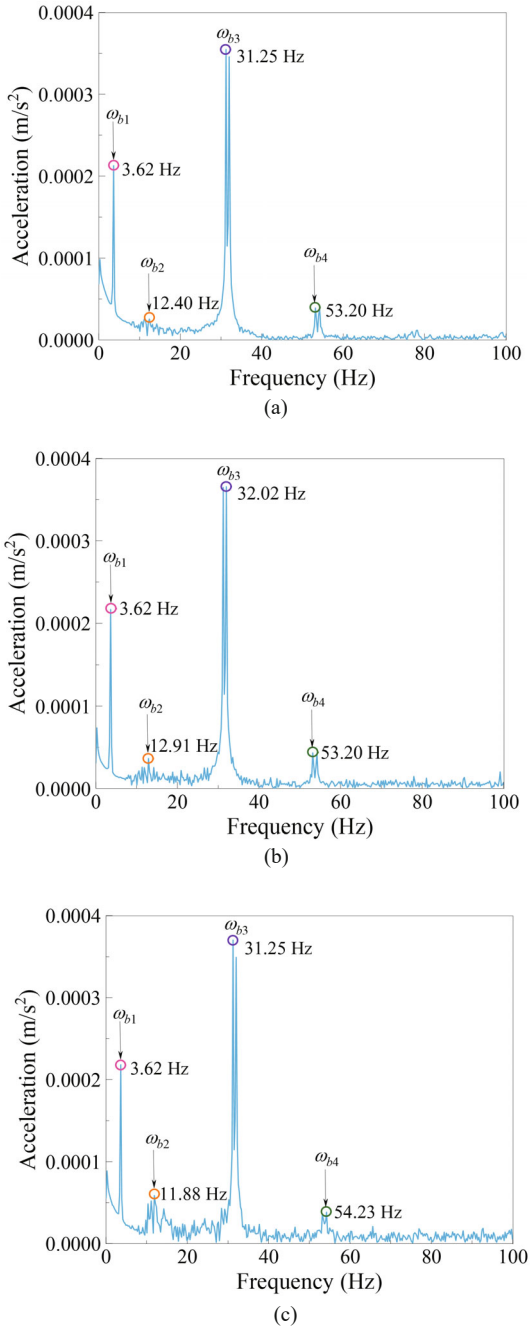

Fig. 4 CP residual spectrum under various classes of road roughness: (a) Class A, (b) Class B, (c) Class C

3.2.4 Effect of bridge type

The applicability of the proposed method was further explored through the BF identification of a three-span continuous bridge (see Table 6 for its properties). As a result, the first six BFs were successfully identified with errors less than 4%, as shown in Table 7. Therefore, the proposed BF identification method is considered applicable to continuous bridges as well.

4 Experimental validation

To verify the effectiveness of the proposed VSM for BF identification, a series of experiments was performed. The vehicle model parameters were first identified in a laboratory experiment, following which a calibration test was performed to validate the accuracy of the smartphone gyroscope in measuring the angular velocity. Finally, a VBI test was performed to identify the BFs.

4.1 Experimental setup

4.1.1 Bridge model

The laboratory setup of the bridge model comprises three components: acceleration zone, test zone, and deceleration zone, as shown in Fig. 5(a). The test zone is a simply supported steel beam that is supported by a hinge at one end and a roller at the other end, as shown in Figs. 5(b) and 5(c), respectively. Two wooden tracks (see Fig. 5(a)) are glued to the top surface of this beam

Table 6 Properties of continuous bridge model

Parameter	Bridge span (m)	Density (kg/m³)	Moment of inertia (m⁴)	Elastic modulus (GPa)
Value	3 × 30	2700	11.13	34.5

Table 7 Comparison of identified and theoretical BFs (unit: Hz)

BF	Identified	Theory	Error
1st BF	3.644	3.630	0.39%
2nd BF	4.677	4.651	0.56%
3rd BF	6.830	6.789	0.60%
4th BF	14.175	14.439	1.83%
5th BF	16.100	16.451	2.13%
6th BF	19.51	20.167	3.26%

to guide the vehicle movement. Figure 5(d) shows the cross-sectional dimensions of the bridge test zone, and Table 8 lists its properties. The bridge model has a smooth surface, implying that the road roughness is not considered in this experiment.

4.1.2 Model car

In the experiment, a two-axle (four-DOF) model car is used (see Fig. 6(a)). The model car comprises three main components: rubber wheels, suspension system, and body. A smartphone (Redmi K30 Pro) is mounted at the center of the car body to obtain its responses (i.e., vertical acceleration along the z-axis and angular velocity around the x-axis) when passing over the test zone via the built-in acceleration sensor and gyroscope, respectively. Due to the limitations of the equipment at hand, the model car is pulled along the track at a constant speed of 0.08 m/s by the traction system (see Fig. 6(b)).

4.2 Model car parameter identification

As discussed in Section 2, to obtain the vehicle CP response from the body response, accurate physical parameters of the vehicle model are required; these should be obtained before BF identification. Because the model car is symmetric, only six of the parameters listed in Table 2 must be identified: k_1, k_3, c_1, m_v, m_1, and I_v.

Figure 7 shows the experimental setup for identifying the parameters of the model car. Here, the model car is stationary on the bridge test zone, and two INV9822A

Table 8 Bridge test zone properties

Span (m)	Density (kg/m^3)	Cross-sectional area (mm^2)	Moment of inertia (mm^4)	Elastic modulus (GPa)
3	7800	2690	39586	206

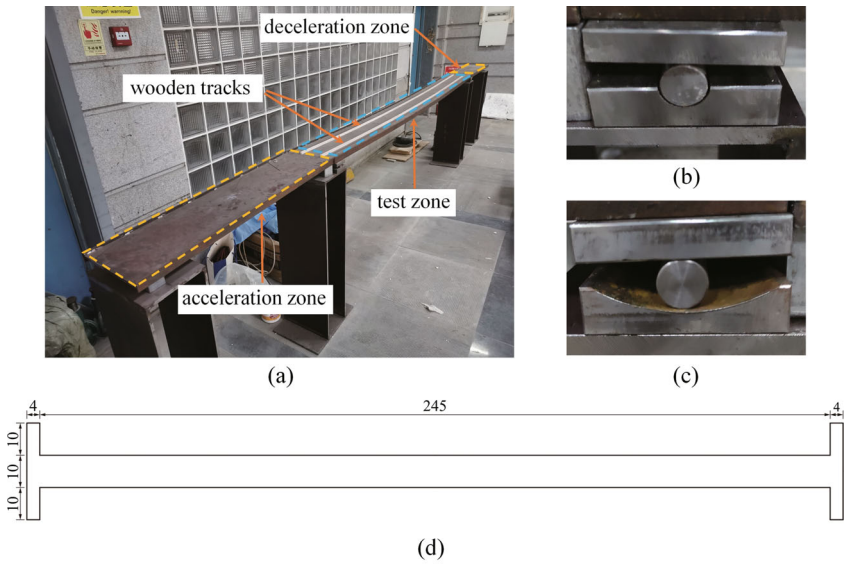

Fig. 5 Experimental beam bridge model: (a) experimental setup, (b) hinge support, (c) roller support, and (d) beam cross-section (unit: mm)

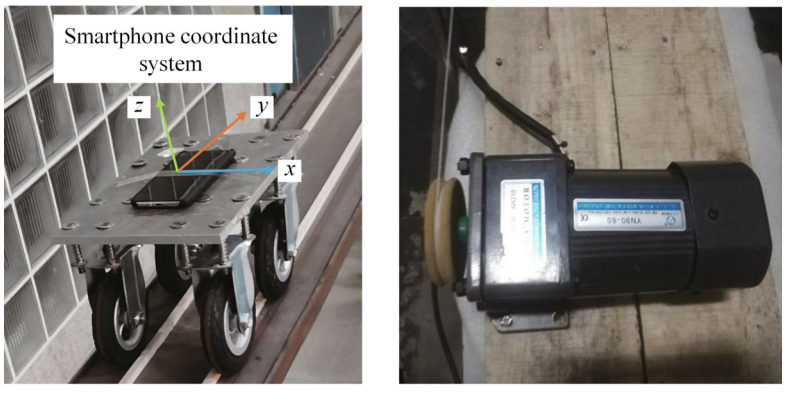

Fig. 6 (a) Instrumentation on model car mounted with smartphone and (b) traction system

piezoelectric accelerometers (COINV) are mounted at two points on its body (i.e., points A and B shown in Fig. 2) to measure its vertical acceleration. Then, the CP acceleration can be calculated using the obtained body response and model car parameters. Another accelerometer of the same type is used to measure the acceleration of the bridge surface (center between two front wheels); this is considered as the actual CP acceleration herein. An INV3060A data acquisition instrument (COINV) is used for obtaining acceleration data. The bridge surface is excited by striking it with a hammer, and the sampling frequency of the accelerometers is set as 200 Hz.

A genetic algorithm (GA) is used for optimizing the model car parameters, wherein an objective function is set to minimize the difference between the measured and calculated CP responses in the frequency domain, as shown in Eq. (15). Furthermore, to prevent local convergence, the above-described vibration test is performed three times, and the GA is applied three times for each test. Vehicle parameter identification using a GA is described in detail elsewhere (Zhao *et al*., 2017, 2019). Table 9 lists the identified model car parameters according to the smallest GA objective-function value. These parameters were used for the following BF identification. To this end, the vehicle/bridge mass ratio is around 2%, which is close to the mass ratio in the numerical simulation (1.72%).

$$C=\sqrt{\frac{\int\left\{\hat{S}_{\mathrm{acc}}(f)-S_{\mathrm{acc}}(f)\right\}\mathrm{d}f}{\int S_{\mathrm{acc}}(f)\mathrm{d}f}} \tag{15}$$

where $\hat{S}_{\mathrm{acc}}(f)$ and $S_{\mathrm{acc}}(f)$ denote the power spectra density of the calculated and measured CP acceleration, respectively.

Fig. 7 Instrumentation on model car and bridge model with accelerometers

4.3 Smartphone test

4.3.1 Sampling frequency correction

As mentioned earlier, the developed VSM is incorporated into a self-developed Android App for realizing convenient BF identification. Previous studies (Mei and Gül, 2019; Ozer *et al*., 2017) have noted that the sampling frequency of smartphone-embedded sensors typically fluctuates over time. To address this issue, this study uses linear interpolation to acquire data at equal time intervals. After correction, the sampling frequencies of both the acceleration sensor and the gyroscope are set as 200 Hz in the BF identification experiment.

4.3.2 Smartphone gyroscope calibration

The performance of smartphone-embedded acceleration sensors has been widely investigated (Mei and Gül, 2019; Ozer *et al*., 2017). However, few studies have investigated the angular velocity measurement accuracy of a smartphone gyroscope. Therefore, a laboratory calibration test was performed to identify the reliability of the smartphone gyroscope for angular velocity measurements.

A previous study (Yu and Lubineau, 2021) indicated that the performance of the built-in gyroscope of a smartphone for measuring rotations around three axes (i.e., pitch, roll, and yaw rotation) is similar. Therefore, for simplicity, a rotation test was performed around the *z*-axis alone. The smartphone was fixed on the motor to enable its rotation along the *z*-axis, as shown in Fig. 8. A variable frequency governor was used to adjust the angular velocity of the motor, and the four velocity values — 1.3, 1.7, 2.1, and 2.5 rad/s — were verified.

For the sake of brevity, only partial gyroscope data at 1.3 rad/s test velocity are presented herein as an example, as shown in Fig. 9(a). The smartphone also collects some anomalous angular velocity data around zero, thereby disturbing the angular acceleration significantly (e.g., up

Table 9 Identified model car parameters

Parameter	k_1 (N/m)	k_3 (N/m)	c_1 (N·s/m)	m_v (kg)	m_1 (kg)	I_v (kg·m^2)
Value	32034	595	142	0.646	0.214	0.008

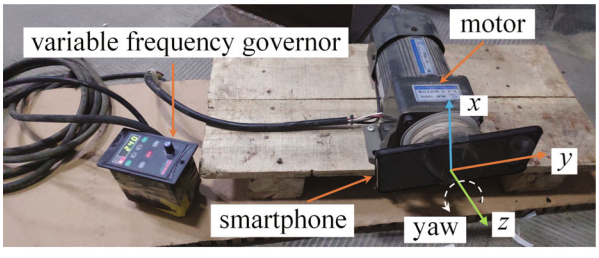

Fig. 8 Experimental arrangement for smartphone gyroscope calibration

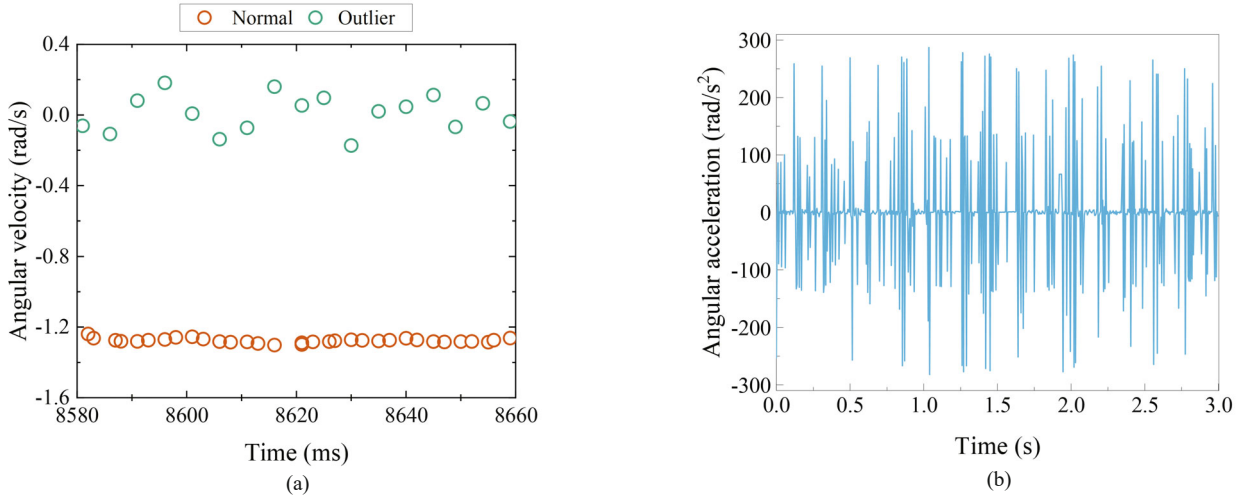

Fig. 9 Smartphone gyroscope data at 1.3 rad/s test velocity: (a) angular velocity and (b) angular acceleration

to 300-500 rad/s^2, as shown in Fig. 9(b)) and affecting the accuracy and reliability of the BF identification results. This phenomenon also exists in other cases. In this study, the angular velocity outliers in the original data were identified and filtered using the criteria shown in Eq. (16). For example, the angular velocity data shown in Fig. 9(a) has the standard deviation of 0.613. Therefore, the threshold was set as 0.01 rad/s, and the filtered data only has the standard deviation of 0.013, indicating that the outliers were removed successfully.

$$\begin{aligned} \left|x(i)-x(i-1)\right| &\geq x_0 \\ \left|x(i)-x(i+1)\right| &\geq x_0 \end{aligned} \tag{16}$$

Here, $x(i)$ denotes the ith value and x_0 denotes the threshold selected based on the standard deviation of the measured data.

4.4 BF identification results

4.4.1 Measurement using modal test

To offer a reference for comparison with the BF identification results obtained using the model car, a modal test was conducted on the bridge model excited by being struck with a hammer for BF identification. Four INV9822A piezoelectric accelerometers were mounted on the bridge surface evenly and used to measure the dynamic responses of the bridge, as shown in Fig. 10. The INV3060A data acquisition instrument (COINV) is used for this purpose. The sampling frequency is 200 Hz. The first four BFs obtained are 3.711, 14.650, 32.810, and 58.200 Hz.

4.4.2 Measurement using model car

Figure 11(a) shows the body responses of the model car as it passes over the bridge test zone, and Fig. 11(b) shows the BF identification results derived from the

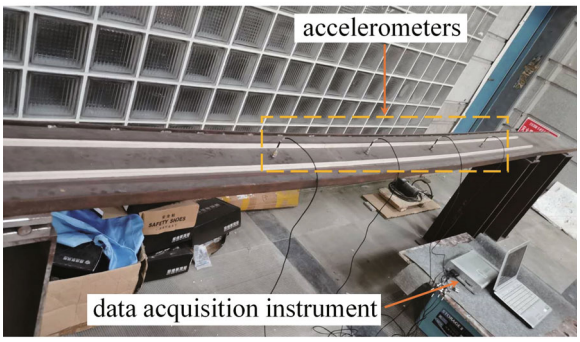

Fig. 10 Experimental setup of modal test

smartphone App. The first two BFs (i.e., 3.399 and 13.564 Hz, respectively) are seen to be identified clearly; these are lower than the modal test results with an error of ~8%. Figure 11(b) also shows that the third- and higher-mode BFs are masked by environmental noise, implying that the proposed method is sensitive to noise; this issue should be addressed in future studies. The experimental results indicate that the proposed VSM can be used to identify the first two BFs with acceptable accuracy.

5 Conclusions

This study proposes a smartphone-based BF identification method that uses the CP acceleration response of a four-DOF vehicle model and verifies its effectiveness through both numerical and experimental investigations. Extensive numerical studies are performed to evaluate the accuracy and robustness of the proposed VSM in various situations. To demonstrate its practical implementation, the proposed BF identification method has been incorporated into a self-developed smartphone app to facilitate smooth data collection and timely BF identification. Furthermore, the proposed strategy can be extended to monitor the operational behaviors of several

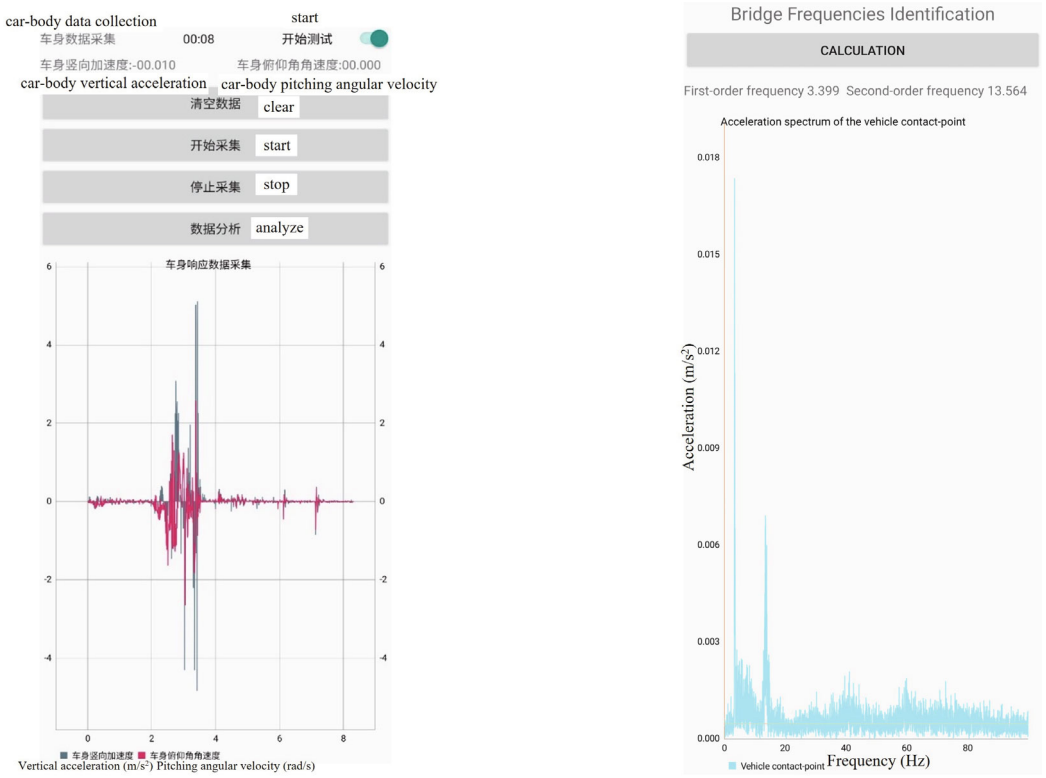

(a) (b)

Fig. 11 BF identification using model car equipped with smartphone: (a) data collection and (b) BF identification result

bridges using crowdsourced smartphone data. The major conclusions drawn from this study are listed below.

(1) The numerical investigations indicate that the proposed VSM works well for a range of vehicle speeds and spans of a simply supported bridge. In addition, this method can be applied to a continuous bridge.

(2) The effect of road roughness on BF identification can be successfully eliminated by using the CP acceleration residual spectrum.

(3) The gyroscope measurements may contain anomalous data; therefore, such data must first be filtered out to ensure the reliability of the obtained data.

(4) In the field experiments, the effect of road roughness is not considered. By using the above-described experimental equipment and the proposed method, the first two BFs for a simply supported bridge can be retrieved with acceptable accuracy (i.e., ~8%).

In summary, the above results indicate that the proposed smartphone-based drive-by inspection method could be used for the rapid BF identification of short- and medium-span simply supported and continuous bridges. Future studies will aim to verify the proposed method through field experiments and enhance its robustness using crowdsourced data, making it possible to monitor the operational frequency of a larger population of bridges simultaneously and in almost real time. However, in the present experiments, the speed of the model car is rather low (i.e., 0.08 m/s) to guarantee the sampling quality. Moreover, performing further study considering BF identification under higher speeds to improve the measurement efficiency, and investigating the effect of vehicle mass will shed more light on the potential benefit of this BF identification method. Finally, experimental results reveal that the proposed method could be sensitive to environmental noise; future studies must address this issue.

References

ANSYS (2021), *ANSYS User's Manual Version 17.0*, Houston, USA: ANSYS Inc.

Cantero D, Hester D and Brownjohn J (2017), "Evolution of Bridge Frequencies and Modes of Vibration During Truck Passage," *Engineering Structures*, **152**: 452–464.

Cantero D, McGetrick P, Kim CW and Obrien E (2019), "Experimental Monitoring of Bridge Frequency Evolution During the Passage of Vehicles with Different Suspension Properties," *Engineering Structures*, **187**: 209–219.

Chen Y and Feng MQ (2003), "A Technique to Improve the Empirical Mode Decomposition in the Hilbert-Huang Transform," *Earthquake Engineering and Engineering Vibration*, **2**(1): 75–85.

Han J, Zheng P and Wang H (2014), "Structural Modal Parameter Identification and Damage Diagnosis Based on Hilbert-Huang Transform," *Earthquake Engineering and Engineering Vibration*, **13**(1): 101–111.

ISO-8608 (1995), *Mechanical Vibration - Road Surface*

Profiles - Reporting of Measured Data, International Organization for Standardization.

Jian XD, Xia Y and Sun LM (2020), "An Indirect Method for Bridge Mode Shapes Identification Based on Wavelet Analysis," *Structural Control and Health Monitoring*, **27**(12): e2630.

Jin N, Yang YB, Dimitrakopoulos EG, Paraskeva TS and Katafygiotis LS (2021), "Application of Short-Time Stochastic Subspace Identification to Estimate Bridge Frequencies from a Traversing Vehicle," *Structural Control and Health Monitoring*, **230**: 111688.

Li J, Zhu XQ, Law SS and Samali B (2019a), "Indirect Bridge Modal Parameters Identification with One Stationary and One Moving Sensors and Stochastic Subspace Identification," *Journal of Sound and Vibration*, **446**: 1–21.

Li J, Zhu XQ, Law SS and Samali B (2019b), "Drive-By Blind Modal Identification with Singular Spectrum Analysis," *Journal of Aerospace Engineering*, **32**(4): 04019050.

Lin CW and Yang YB (2005), "Use of a Passing Vehicle to Scan the Fundamental Bridge Frequencies: An Experimental Verification," *Engineering Structures*, **27**(13): 1865–1878.

Matarazzo TJ, Santi P, Pakzad SN, Carter K, Ratti C, Moaveni B, *et al.* (2018), "Crowdsensing Framework for Monitoring Bridge Vibrations Using Moving Smartphones," *Proceedings of the IEEE*, **106**(4): 577–593.

Mei Q and Gül M (2019), "A Crowdsourcing-Based Methodology Using Smartphones for Bridge Health Monitoring," *Structural Health Monitoring*, **18**(5–6): 1602–1619.

Mei Q, Gül M and Boay M (2019), "Indirect Health Monitoring of Bridges Using Mel-Frequency Cepstral Coefficients and Principal Component Analysis," *Mechanical Systems and Signal Processing*, **119:** 523–546.

Mei Q, Gül M and Shirzad-Ghaleroudkhani N (2020), "Towards Smart Cities: Crowdsensing-Based Monitoring of Transportation Infrastructure Using in-Traffic Vehicles," *Journal of Civil Structural Health Monitoring*, **10**(4): 653–665.

Nagarajaiah S and Basu B (2009), "Output Only Modal Identification and Structural Damage Detection Using Time Frequency & Wavelet Techniques," *Earthquake Engineering and Engineering Vibration*, **8**(4): 583–605.

Ozer E, Feng D and Feng MQ (2017), "Hybrid Motion Sensing and Experimental Modal Analysis Using Collocated Smartphone Camera and Accelerometers," *Measurement Science and Technology*, **28**(10): 105903.

Paraskeva TS, Dimitrakopoulos EG and Zeng Q (2017), "Dynamic Vehicle–Bridge Interaction Under Simultaneous Vertical Earthquake Excitation," *Bulletin of Earthquake Engineering*, **15**(1): 71–95.

Shirzad-Ghaleroudkhani N and Gül M (2020), "Inverse Filtering for Frequency Identification of Bridges Using Smartphones in Passing Vehicles: Fundamental Developments and Laboratory Verifications," *Sensors*, **20**(4): 1190.

Shirzad-Ghaleroudkhani N, Mei Q and Gül M (2020), "Frequency Identification of Bridges Using Smartphones on Vehicles with Variable Features," *Journal of Bridge Engineering*, **25**(7): 04020041.

Shokravi H, Shokravi H, Bakhary N, Heidarrezaei M, Rahimian Koloor SS and Petrů M (2020), "Vehicle-Assisted Techniques for Health Monitoring of Bridges," *Sensors*, **20**(12): 3460.

Yang YB, Chang CH and Yau JD (1999), "An Element for Analysing Vehicle-Bridge Systems Considering Vehicle′s Pitching Effect," *International Journal for Numerical Methods in Engineering*, **46**(7): 1031–1047.

Yang YB and Chang KC (2009), "Extraction of Bridge Frequencies from the Dynamic Response of a Passing Vehicle Enhanced by the EMD Technique," *Journal of Sound and Vibration*, **322**(4–5): 718–739.

Yang YB, Chang KC and Li YC (2013b), "Filtering Techniques for Extracting Bridge Frequencies from a Test Vehicle Moving over the Bridge," *Engineering Structures*, **48**: 353–362.

Yang YB, Chen WF, Yu HW and Chan CS (2013a), "Experimental Study of a Hand-Drawn Cart for Measuring the Bridge Frequencies," *Engineering Structures*, **57**: 222–231.

Yang YB, Li YC and Chang KC (2012), "Using Two Connected Vehicles to Measure the Frequencies of Bridges with Rough Surface: A Theoretical Study," *Acta Mechanica*, **223**(8): 1851–1861.

Yang YB, Lin CW and Yau JD (2004), "Extracting Bridge Frequencies from the Dynamic Response of a Passing Vehicle," *Journal of Sound and Vibration*, **272**(3–5): 471–493.

Yang YB, Wang BQ, Wang ZL, Shi K and Xu H (2022), "Scanning of Bridge Surface Roughness from Two-Axle Vehicle Response by EKF-UI and Contact Residual: Theoretical Study," *Sensors*, **22**(9): 3410.

Yang YB, Wang ZL, Shi K, Xu H and Wu YT (2020a), "State-of-the-Art of Vehicle-Based Methods for Detecting Various Properties of Highway Bridges and Railway Tracks," *International Journal of Structural Stability and Dynamics*, **20**(13): 2041004.

Yang YB, Xu H, Zhang B, Xiong F and Wang ZL (2020b), "Measuring Bridge Frequencies by a Test Vehicle in Non-Moving and Moving States," *Engineering Structures*, **203:** 109859.

Yang YB and Yang JP (2018), "State-of-the-Art Review on Modal Identification and Damage Detection of Bridges by Moving Test Vehicles," *International Journal of Structural Stability and Dynamics*, **18**(2): 1850025.

Yang YB, Yang JP, Zhang B and Wu YT (2019a), *Vehicle Scanning Method for Bridges*, first ed. Hoboken: Wiley, USA.

Yang YB and Yau JD (2015), "Vertical and Pitching Resonance of Train Cars Moving over a Series of Simple Beams," *Journal of Sound and Vibration*, **337**: 135–149.

Yang YB, Zhang B, Chen YA, Qian Y and Wu YT (2019b), "Bridge Damping Identification by Vehicle Scanning Method," *Engineering Structures*, **183**: 637–645.

Yang YB, Zhang B, Qian Y and Wu YT (2018), "Contact-Point Response for Modal Identification of Bridges by a Moving Test Vehicle," *International Journal of Structural Stability and Dynamics*, **18**(5): 1850073.

Yang YB, Zhang B, Wang T, Xu H and Wu Y (2019c), "Two-Axle Test Vehicle for Bridges: Theory and Applications," *International Journal of Mechanical Sciences*, **152**: 51–62.

Yu LP and Lubineau G (2021), "A Smartphone Camera and Built-in Gyroscope Based Application for Non-Contact Yet Accurate Off-Axis Structural Displacement Measurements," *Measurement*, **167:** 108449.

Zeng Q, Liu CY, Duan ZD, Yang JZ, Chen T and Wang S (2022), "An Algebraic Elimination by Substitution Algorithm for Vehicle–Bridge Interaction Problems," *International Journal of Structural Stability and Dynamics*, 2250176.

Zhao BY and Nagayama T (2017), "IRI Estimation by the Frequency Domain Analysis of Vehicle Dynamic Responses," *Procedia Engineering*, **188**: 9–16.

Zhao BY, Nagayama T and Xue K (2019), "Road Profile Estimation, and Its Numerical and Experimental Validation, by Smartphone Measurement of the Dynamic Responses of an Ordinary Vehicle," *Journal of Sound and Vibration*, **457**: 92–117.